Design and Analysis of a Novel Hybrid Excitation Flux Reversal Machine

Xianming Deng, Zhen Jia, and Xiaohan Zhao

Jiangsu Province Laboratory of Mining Electric and Automation, China University of Mining and Technology
Xuzhou, 221116, China
xmdengcumt@126.com, TS19130046A31@cumt.edu.cn

Abstract ─ A novel hybrid excitation flux reversal machine (HEFRM) is developed. The machine has a simple reluctance rotor and a stator, which has both an ac armature winding and a dc field winding. The core on the surface of the pole arc at the centerline of the stator pole and the core on the outer surface of the stator yoke each have a slot along the rotating axis, where the field windings are placed. A permanent magnet (PM) with opposite polarity is placed respectively on each side of a slot in the same stator pole. In this paper, the working principle of the new HEFRM is introduced, the influence of magnetic pole parameters and armature parameters on motor performance are also analyzed, and genetic algorithm (GA) is used for multi-objective optimization of the torque characteristics. Finally, the HEFRM prototype is built, and its theoretical correctness is verified by the finite element analysis (FEA).

Index Terms ─ FEA, flux-reverse machine, GA, hybrid excitation, multi-objective optimization.

I. INTRODUCTION

Flux-reverse machine (FRM) is a new type of machine, in which rare-earth PMs are added to the stator or the surface of pole shoes of a switched reluctance machine (SRM). Because of its high power density, small rotational inertia, compact structure, easy to install, and other performance advantages, the application prospects are very broad, it can be used in automotive power generation, power tools, industrial drive, and other fields [1-4]. Since the end of the last century, the single-phase and three-phase FRM has been proposed [5], and many new types of FRM have been developed as a result of extensive research on the structure of the FRM, such as double stator flux reversal machine [6], flux reversal linear machine [7-9], Halbach permanent magnet flux reversal machine [10] and hybrid excitation flux reversal machine [11].

HEFRM has two different magnetomotive force sources, the air gap main magnetic field is established by permanent magnets and the electric excitation plays an auxiliary role. Thus, the PM machine can be combined with the electric excitation machine organically [12-14]. When operating as a motor, the speed range of the motor is extended; when operating as a generator, the output voltage can be adjusted to improve the quality of the power supply. The HEFRMs are promising candidates for many areas especially for direct-drive systems requiring a wide speed range. Thus, it is of high research value and practical significance.

In this paper, a new type of hybrid excitation flux reversal permanent magnet machine is proposed. Meanwhile, the FEA is used to analyze its performance, and achieve its modulation of the air-gap magnetic field. By comparison, it is verified that it can achieve a wider speed range and better overload capability.

II. STRUCTURE AND WORKING PRINCIPLE

The basic structure of the traditional flux reversal machine is shown in Fig. 1. It consists of four basic parts: the armature winding, the permanent magnet, the field winding, and the rotor as a magnetic flux modulator. The PM magnetomotive force (MMF) of the traditional flux reversal machine is basically unchanged during operation. In vector control, to run the machine above the base speed, the only way is to adjust the direct axis current to attenuate the magnetic field for flux weakening speed regulation. However, the torque performance of the machine will inevitably be wakened. Therefore, to better achieve magnetic field regulation, a novel hybrid excitation flux reversal machine is proposed in this paper, as shown in Fig. 1 (a).

Compared with the traditional flux reversal machine, in the structure of the HEFRM, along the rotating axis, there is a field winding slot not only on the core of the pole arc surface at the centerline of the stator pole, but also on the core of the outer surface of the stator yoke. The DC field winding is in the form of concentrated winding, which is alternately wound in the field winding slot, as shown in Fig. 1. The structure of the power winding is the same as that of a normal winding. The power winding is placed in the stator slot, which is orthogonal to the field winding in space. A PMs is placed on both sides of each stator pole shoe of the machine. Each PM is opposite in polarity to a PM on the same

Submitted On: August 22, 2020
Accepted On: January 18, 2021

https://doi.org/10.47037/2020.ACES.J.360215

tooth and identical in polarity to a PM on an adjacent tooth. For the application of the new structure, the HEFRM and the traditional flux reversal machine have the same arrangement of PMs and the same number of pole pairs. So, the structure and operating principle of the two machines are very similar, which greatly simplifies the theoretical analysis and design of the new machine.

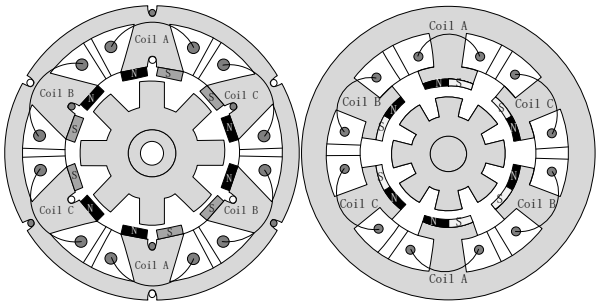

Fig. 1. (a) Basic structure diagram of hybrid excitation flux reversal permanent magnet machine, and (b) basic structure diagram of traditional flux reversal permanent magnet machine.

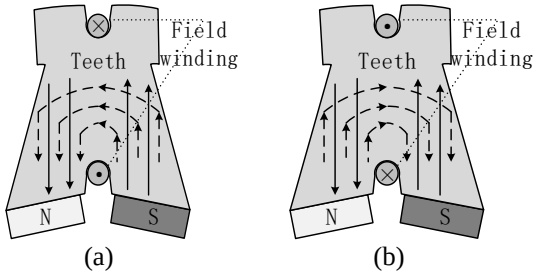

Fig. 2. Flux linkage of a stator tooth: (a) turn on the flux enhancement current, and (b) turn on the flux weakening current.

In general, the field winding is connected with demagnetization current to conduct flux weakening speed regulation. As shown in Fig. 2 (b), after the flux weakening current is applied, the magnetic field of the field winding forms a loop through the stator teeth. This loop is connected in series with the permanent magnet magnetic circuit. When the flux of the field winding passes through the permanent magnet, which is in danger of demagnetization if not properly controlled. As shown in Fig. 2 (a), if demagnetization of a PM occurs, the current opposite to demagnetization can be applied, in that PM can be magnetized to improve system reliability. Since the field winding is spatially orthogonal to the power winding, the two are decoupled. As shown in the Fig. 3, when the power winding is applied a sinusoidal voltage, the induced electromotive force of the field winding on the same tooth is very weak. Without considering the effect of armature current on excitation current, this characteristic makes it possible to simplify the control strategy in weak magnetic control. Moreover, the field winding is placed in a special slot instead of in the stator slot. This design makes the field winding does not occupy the stator slot area with the armature winding. It also does not weaken the electrical load and synchronous reactance of the armature windings by increasing the field winding. Therefore, the design of the machine can be further simplified.

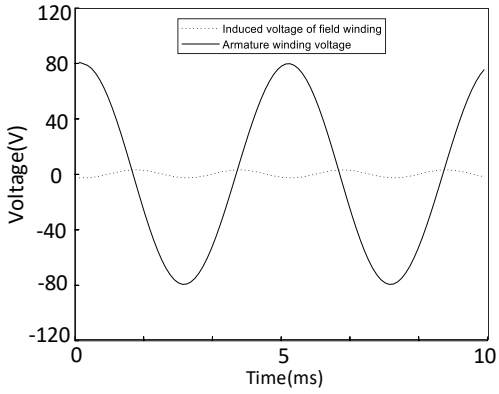

Fig. 3. Induced electromotive force of field winding when armature winding is electrified.

The working principle of HEFRM is similar to that of traditional flux reversal machine, which belongs to the family of flux modulation machines. Magnetic flux modulation machine armature winding pole number P_a and magnetic field rotation angular velocity Ω_a meet the requirements:

$$\begin{cases} P_a = |P_e - P_m| \\ \Omega_a = (P_e\Omega_e - P_m\Omega_m)/(P_e - P_m) \end{cases}, \quad (1)$$

where Ω_e and Ω_m are MMF of the permanent magnet and the angular velocity of the rotor, P_e and P_m are the numbers of poles of PM and the period number of flux modulator, in FRM $P_m = Z_r/2$, Z_r is the number of rotor slots. To place the three-phase winding, the number of stator slots and the number of armature winding poles shall be satisfied:

$$Z_s = 3kP_a, k = 1,2,3\cdots. \quad (2)$$

From the above analysis, the commonly used pole slot combinations of HEFRM are shown in Table 1.

Table 1: Pole slot combinations of HEFRM

Z_s	Z_r	2	4	5	7	8	10	11
6	P_a	1	1	2	2	1	1	2
	SPP	1	1	0.5	0.5	1	1	0.5
	GR	2	4	2.5	3.5	8	10	5.5
12	P_a	4	2	1	1	2	4	5
	SPP	0.5	1	2	2	1	0.5	0.4
	GR	0.5	2	5	7	4	2.5	2.2

PS: SPP is the number of slots per pole per phase, GR is gear ratio (Ratio of rotor slot number Z_r to winding pole number P_a).

Taking 6-stator-slot / 8-rotor-slot HEFRM as an example, the distribution of the magnetic force line of HEFRM is shown in Fig. 3. As can be seen from this figure, whether the PMs are excited individually or the field windings are excited individually, when the rotor rotates a rotor slot distance, the flux linkage of the A-phase windings are reversed. Therefore, the operation principle of HEFRM is the same as that of traditional FRM. Due to the use of hybrid excitation, the working flux density of the PM B_m is determined by the joint action of the residual magnetic field of the PM B_r and applied magnetic field exerted on the PM by the excitation coil and the armature winding together H_m:

$$B_m = B_r + \mu_0\mu_{rm}H_m \,, \tag{3}$$

where μ_{rm} is the relative permeability of PM. The external MMF is equal to the magnetic pressure drop of the air gap and PM. Ignoring the magnetic pressure drop of the core, the MMF of the whole magnetic circuit can be expressed as:

$$H_m l_m + H_g l_g = N_{dc}I_{dc} + N_{ac}I_{ac} \,, \tag{4}$$

where NI is the MMF of the external field winding, l_m and l_g is the thickness of PM and the length of air gap, respectively. H_g is the air gap magnetic field strength. In the air gap, the flux density of magnetic field strength can be expressed as:

$$B_g = \mu_0 H_g \,. \tag{5}$$

Besides, both air gap flux φ_g and permanent magnetic flux φ_m can be expressed as the multiplication of flux density and cross-sectional area:

$$\begin{cases} \varphi_g = B_g A_g \\ \varphi_m = B_m A_m \end{cases}, \tag{6}$$

introducing the magnetic flux leakage coefficient k,

$$\varphi_g = \frac{\varphi_m}{k} \,. \tag{7}$$

Substituting (4) - (7) into (3) can be obtained:

$$B_m = \frac{1}{1+\mu_{rm}\frac{A_m l_g}{A_g l_m K}}\left[B_r + \mu_0\mu_{rm}\frac{N_{dc}I_{dc}+N_{ac}I_{ac}}{l_m}\right] . \tag{8}$$

From the above equation, it can be seen that the operating magnetic density of a permanent magnet can be increased or decreased by changing the direction of the incoming excitation current. Due to the slotting of the rotor, the air gap length of the machine is not fixed but varies periodically with the circumferential position angle θ_s and the rotor position angle θ. The air gap flux density $\mathrm{B}(\theta_s, \theta)$ can be expressed as the product of the MMF $F_m(\theta_s)$ and the air gap permeability function $\Lambda(\theta, \theta_s)$:

$$\mathrm{B}(\theta_s, \theta) = F_m(\theta_s)\Lambda(\theta, \theta_s) \,. \tag{9}$$

The distribution of the magnetic field lines of the machine is shown in Fig. 4.

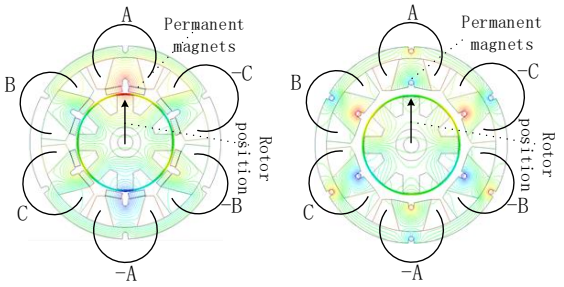

Fig. 4. Distribution of magnetic field lines under different excitation modes: (a) separate excitation of permanent magnet, and (b) the field winding is separately excited.

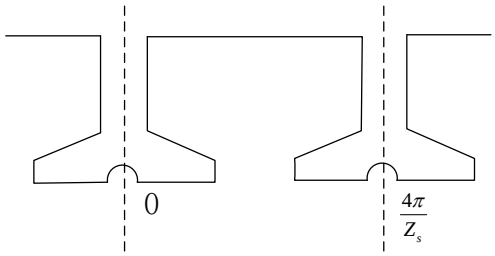

Fig. 5. Distribution of magnetic force lines in different rotor positions.

The structure and PM arrangement of HEFRM are shown in Fig. 6. and the stator slot centerline at position 0, as shown in Fig. 5, the MMF $F_m(\theta_s)$ is an odd function with period $\mathrm{T} = 4\pi/Z_s$:

$$F_m(\theta_s) = \sum_{n=1,3,5\cdots}^{\infty} F_n sin\left(\frac{nZ_s\theta_s}{2}\right) , \tag{10}$$

where

$$\begin{cases} F_n = \frac{8F_c}{n\pi} sin\left(\frac{n\pi}{2}\right) cos\left(\frac{n\pi(1+S_0+S_1)}{4}\right) sin\left(\frac{n\pi(1-S_0+S_1)}{4}\right), \\ F_c = B_m l_m/\mu_0\mu_{rm} \end{cases} \tag{11}$$

where S_0 is the ratio of stator slot opening width to stator slot spacing; S_1 is the ratio of stator slot opening width

to stator slot width. The slotting diagram of stator and rotor is shown in Fig. 6.

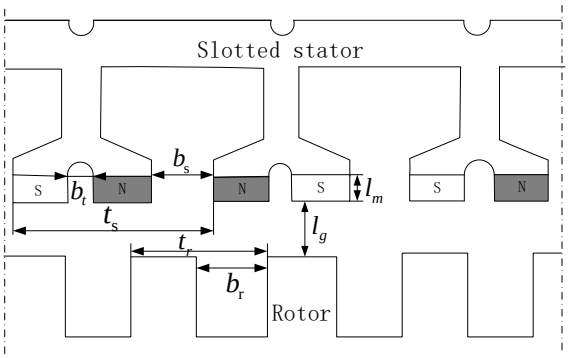

Fig. 6. Slotting diagram of stator and rotor.

As shown in Fig. 5, HEFRM is a typical double salient structure, whose air-gap permeance $\Lambda(\theta,\theta_s)$ can be expressed as the product of the air gap relative permeance $G_r(\theta,\theta_s)$ when the stator is not slotted but the rotor is and the air gap relative permeance $G_s(\theta_s)$ when the stator is slotted but the rotor is not slotted:

$$\Lambda(\theta,\theta_s)=\frac{\mu_0}{l_g}G_r(\theta,\theta_s)G_s(\theta_s), \tag{12}$$

where $G_r(\theta,\theta_s)$ is the air gap relative permeance when the stator is not slotted but the rotor is slotted, and it can be expressed as:

$$G_r(\theta,\theta_s)=\frac{l_m(\theta)}{l_m(\theta)+l_g(\theta,\theta_s)}, \tag{13}$$

where $l_m(\theta)$ and $l_g(\theta,\theta_s)$ respectively represent the distribution of magnetizing direction length and effective air gap length of permanent magnet along circumferential direction when the stator is not slotted and the rotor is slotted. After Fourier decomposition, we can get:

$$G_r(\theta,\theta_s)=G_{r0}+\sum_{i=1,2\cdots}G_{ri}cos[iZ_r(\theta_s-\theta)]. \tag{14}$$

Similarly, $G_s(\theta_s)$ can be expressed as:

$$G_s(\theta_s)=G_{s0}+\sum_{m=1,2\cdots}^{\infty}G_{sm}\cos\left(mZ_s\theta_s\right). \tag{15}$$

To sum up, (9) is rewritten as follows:

$$\mathrm{B}(\theta_s,\theta)=\sum_{\substack{n=1,3,5\cdots\\ i=0,1,2\\ m=0,1,2}}G_{ri}G_{sm}\,F_n sin\left(\frac{nZ_s\theta_s}{2}\right)\cdot$$

$$cos\big(iZ_r\,(\theta_s-\theta)\big)cos(mZ_s\theta_s). \tag{16}$$

Combining (8), (10), (11), and (16), it can be seen that by changing the magnitude and direction of the excitation current, the magnitude of the working magnetic density of the PM can be changed, thus the distribution of MMF of the PM can be changed. Through the modulation of the rotor, a rotating magnetic field can be generated, which directly changes the value of the air gap rotating magnetic field. However, it should be noted that changing the excitation current only changes the amplitude of each harmonic of the air-gap field, and does not introduce new harmonics. The process is shown in Fig. 7.

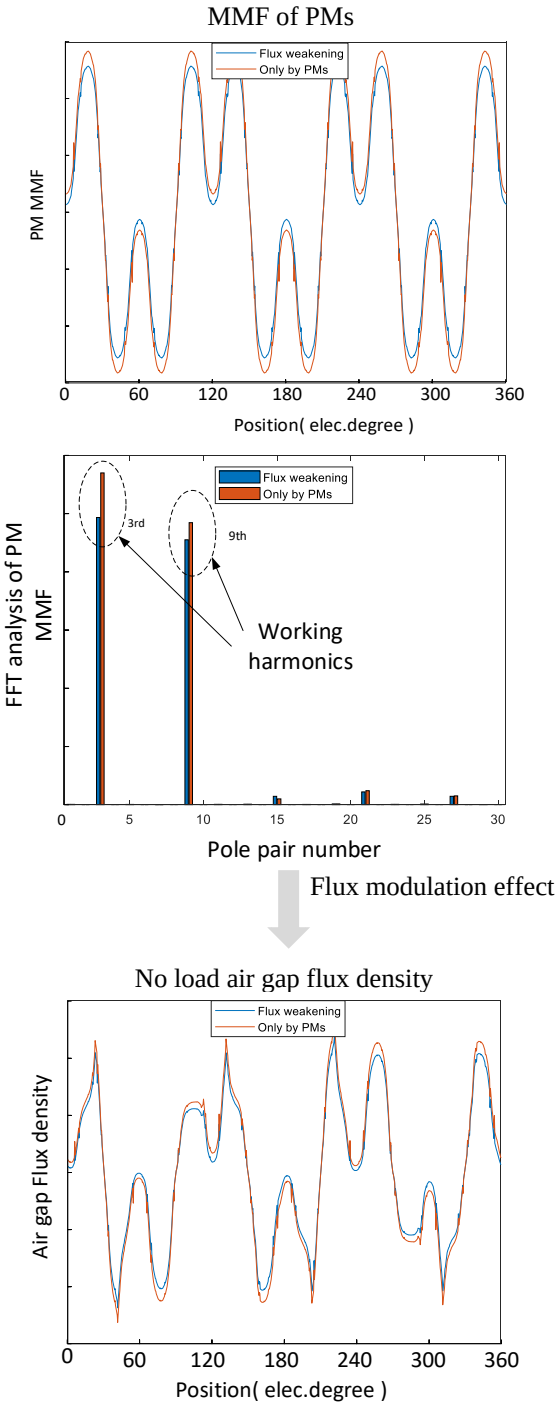

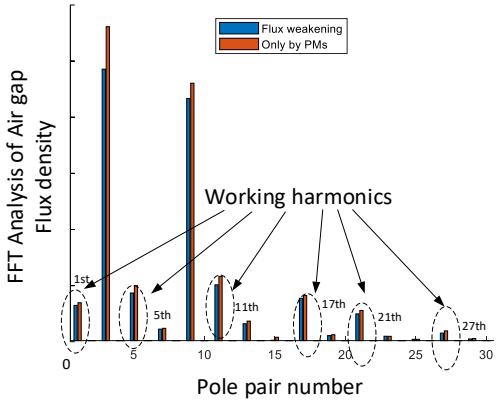

Fig. 7. Comparison of PM MMF and air gap flux density when PM acting alone and flux weakening.

In the analysis of back electromotive force (EMF), to analyze the harmonics of the EMF, the theory of winding function can be applied. The winding function of a three-phase winding is expressed as:

$$\begin{cases} N_a(\theta_s) = \sum_{j=1,3,5\cdots} N_j cos(jP_s\theta_s) \\ N_b(\theta_s) = \sum_{j=1,3,5\cdots} N_j cos\left(jP_s\theta_s - \frac{2}{3}\pi j\right) \\ N_c(\theta_s) = \sum_{j=1,3,5\cdots} N_j cos\left(jP_s\theta_s + \frac{2}{3}\pi j\right) \\ N_j = \frac{2}{j\pi}\frac{N_s}{P_s}K_{wj} \end{cases}, \quad (17)$$

where N_j is the peak value of the jth harmonic of the winding function, N_s is the number of turns in series of each phase, K_{wj} is the winding factor of the jth harmonic and P_s is the pole number of armature winding. The EMF expression of phase A winding can be obtained:

$$e_a(t) = -\frac{d}{dt}\left[r_g l_{stk}\int_0^{2\pi} \mathrm{B}(\theta_s,\theta)N_a(\theta_s)\,d\theta_s\right]\pi\Omega_m \cdot$$

$$r_g l_{stk} Z_r \frac{\mu_0}{l_g}\sum_{\substack{i=\frac{v}{Z_r} \\ j,n,m=1,3,5\cdots}} iG_{ri}G_{sm}F_n N_j cos(iZ_r\theta)\,, \quad (18)$$

where r_g is the radius of the stator inner circle, l_{stk} is the stack length, rotor position angle $\theta = \Omega_m t$, $\mathrm{v} = \frac{(n\pm 2m)Z_s}{2} \pm jP_s$. The comparison of back EMF is shown in Fig. 8.

III. TORQUE PERFORMANCE OPTIMIZATIN DESIGN

Torque density and torque ripple are important performance indexes of FRM. The torque ripple of flux reversal machine is divided into cogging torque caused by stator PMs and rotor harmonic permeance, and torque ripple caused by stator back EMF harmonic and winding current.

In PM machine, cogging torque is inherent. Cogging torque is generated by the harmonic of MMF under the action of higher harmonic of air gap permeance. It is defined as the negative derivative of the magnetic field energy w to the stator-rotor relative position angle θ, when the machine is not energized. It can be expressed as:

$$T_{cog} = -\frac{\partial w}{\partial \theta}, \quad (19)$$

where the magnetic field energy W can be approximately equal to the air gap magnetic field energy W_{gap}:

$$W_{gap} = \frac{1}{2\mu_0}\int_V B(\theta_s,\theta)^2 dV$$

$$= \frac{(R_2^2-R_1^2)l_{stk}}{2\mu_0}\int_0^{2\pi} B(\theta_s,\theta)^2 d\theta_s\,, \quad (20)$$

where R_1 and R_2 are the rotor outer diameter and stator inner diameter respectively. Combined with (16), it can be written as:

$$T_{cog} = \frac{\pi Z_r(R_2^2-R_1^2)l_{stk}}{4l_g}\sum_{i_1\pm i_2=N_p}^{\infty}(i_1 \pm$$

$$i_2)G_{ri_1}G_{ri_2}G_{sm_1}G_{sm_2}F_{n_1}F_{n_2}sin\left(N_p Z_r\theta\right), \quad (21)$$

where

$$N_p = \frac{(n_1\pm n_2\pm m_1\pm m_2)Z_s}{2Z_r}. \quad (22)$$

It can be seen from (21) that the cogging torque is related to the magnetic pole parameters, armature parameters and the number of pole slots of stator and rotor. It can be seen from (22) that not all permeability harmonics will affect cogging torque, and the cogging torque can be reduced by reducing the amplitude of the magnetic pole parameter $F_{n_1}F_{n_2}$ and the armature parameter $\mathrm{G}_{ri_1}\mathrm{G}_{ri_2}G_{sm_1}G_{sm_2}$.

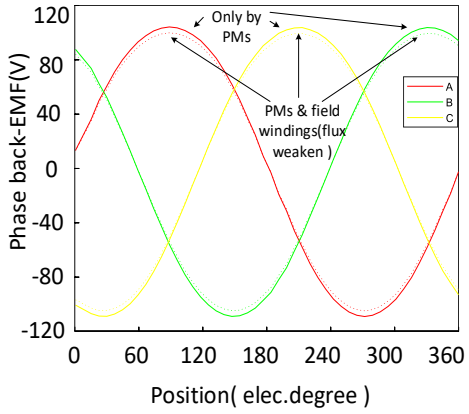

Fig. 8. Comparison of phase back-EMF when PM acting alone and flux weakening.

According to the principle of electromechanical energy conversion, the output torque of three-phase flux reversal machine T_e can be written as:

$$T_e = [e_a(t)i_a(t) + e_b(t)i_b(t) + e_c(t)i_c(t)]/\Omega_m, \quad (23)$$

where $e(t)$ and $i(t)$ are three-phase back EMF and phase current respectively. Combining (17) and (18), (23) can be rewritten as:

$$T_e = \frac{3}{2} i\pi r_g l_{stk} Z_r I_s \frac{\mu_0}{l_g} \cdot \sum_{\substack{i=\frac{v}{Z_r} \\ j,n,m=1,3,5\cdots}} iG_{ri}G_{sm}F_n N_j cos[(i \pm 1)Z_r\theta], \quad (24)$$

where I_s is the peak value of rated current. Take $i, m = 1$, then T_e is equal to the average torque T_{avg}; take $i, m \neq 1$, then T_e is equal to the torque ripple T_r. It can be seen from (24) that, similar to cogging torque, the output torque and torque ripple can also be adjusted by modifying the magnetic pole parameter F_n and armature parameters $G_{ri}G_{sm}$.

Both torque density and torque ripple are affected by the parameters of the magnetic pole and armature. Consequently, in this section, we will use the genetic algorithm combined with the finite element algorithm to design a multi-objective optimization of this machine. From the analysis in the first section, it has been seen that the MMF generated by the field winding only affects the amplitude of the PM working MMF and air gap flux density, and does not change its harmonic content. Therefore, the number of slots for the stator and rotor can be selected in the same way as for the conventional flux reversal machine. In this section, 6-rotor-slot / 8-stator-slot is selected as an example. Its pole ratio is large, and the electromagnetic torque is also relatively large.

A. Design optimization procedure

To optimize the design of the proposed HEFRM, according to the basic structure and working principle of the machine presented in Section II, a prototype has been designed and simulate by FEA. The FEA parameters are shown in Table 2.

For the output torque of the machine, we want greater torque density and smaller torque ripple. Therefore, The objective functions fixed for this optimization are:

-Maximize the average torque of the machine output (T_{avg}),

-Minimize machine torque ripple ($T_{cog} + T_r$).

From the analysis in Section II, the magnetic pole and armature parameters of the machine can be changed by changing stator-rotor slot opening ratio and stator tooth slot opening ratio. Therefore, the optimization parameters are:

-Rotor slot opening ratio (S_2),

-Stator slot opening ratio (S_0),

-Stator tooth slot opening ratio (S_1).

Due to the requirements of mechanical strength and the space for placing the windings. The constraints of the optimization parameters are shown in Table 3.

Table 2: FEA parameters

Parameter	Value	Parameter	Value
Phase number	3	Stator outer diameter	100mm
Rotor slot number	8	Rotor outer diameter	50mm
Stator slot number	6	Air gap length	1mm
Stack length	80mm	PM thickness	3mm
Turns per AC coil	160	PM remanence	1.15T
Turn ratio of dc to ac winding	0.5	Rated speed	1500rpm
Stator tooth slot opening ratio	0.22	Rated frequency	200Hz
Stator slot opening ratio	0.35	Rated ac winding current	5A
Rotor slot opening ratio	0.45	Maximal dc winding current	5A

PS: The rotor slot opening ratio S_2 is defined as $S_2 = b_r/t_r$, where b_r is the rotor slot width and t_r is the rotor slot pitch.

Table 3: Constraints of the optimization parameters

Optimization Parameters	Minimum	Maximum
Rotor slot opening ratio (S_2)	0.4	0.6
Stator slot opening ratio (S_0)	0.2	0.5
Stator tooth slot opening ratio (S_1)	0.2	0.4

Setting the above conditions, the optimization engine uses multi-objective genetic algorithm, the population size is set to 10 times the number of optimization parameters, that is 30, and the maximum number of generations is 65.

B. Optimization results

The optimization of this machine using the multi-objective genetic algorithm took 30 hours, with a total of 1840 model iterations. The Pareto-optimal front of the average torque verse torque ripple of the machine output is obtained, as shown in Fig. 9.

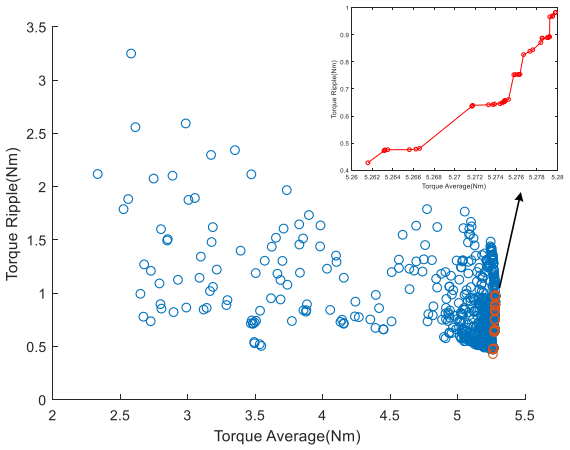

Fig. 9. Pareto-optimal front.

The comparison of optimized parameter values before and after optimization is shown in Table 4, and the comparison of output torque before and after optimization is shown in Fig. 10. As can be seen in Fig. 10, the optimized machine has a larger average torque and smaller torque ripple.

Table 4: Constraints of the optimization parameters

Optimization Parameters	Initial Value	Optimization Values
Rotor slot opening ratio (S_2)	0.45	0.58
Stator slot opening ratio (S_0)	0.35	0.27
Stator tooth slot opening ratio (S_1)	0.22	0.2

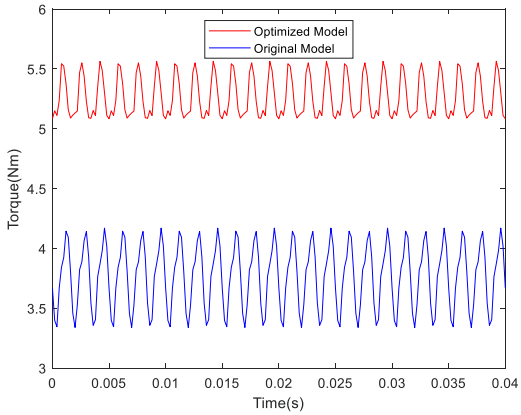

Fig. 10. Comparison of output torque before and after optimization.

The optimization algorithm is based on the results of 2D FEA, considering that the machine contains different active magnetic circuits. We also performed 3D FEA to evaluate the end effect. The open-circuit end effect coefficient E_{eopen} and the on-load end effect coefficient E_{eload} [15] are defined respectively:

$$\begin{cases} E_{eopen} = \frac{E_{3-D}}{E_{2-D}} \times 100\% \\ E_{eload} = \frac{T_{avg3-D}}{T_{avg2-D}} \times 100\% \end{cases}, \tag{25}$$

where E_{eopen} can be defined as the ratio of back EMF E_{3-D} from 3D FEA and the back EMF E_{2-D} from 2D FEA. E_{eload} can be defined as the ratio of the average torque T_{avg3-D} from the 3D FEA and the average torque T_{avg2-D} from the 2D FEA. The result is shown in Fig. 11.

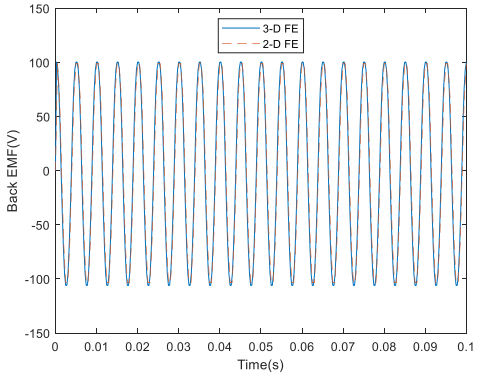

(a) Output torque

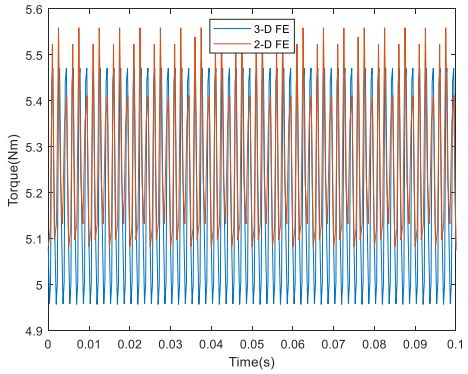

(b) Back EMF

Fig. 11. Comparison between 3D FEA and 2D FEA.

Table 5: End effect coefficient

Project	2D FEA	3D FEA
Average output torque	5.2633Nm	5.1966Nm
E_{eload}	98.7%	
Back EMF amplitude	98.9564V	100.3322V
E_{eopen}	101.4%	

From Table 5, we can see that the end effect coefficients are small. Therefore, we can consider that the optimal model parameters of the machine obtained from 2D FEA are reasonable.

IV. PERFORMANCE ANALYSIS

To analyze the performance of the HEFRM, the machine parameters are shown in Table 6, and its output characteristics are tested.

Table 6: Parameters of HEFRM

Parameter	Value	Parameter	Value
Phase number	3	Stator outer diameter	100mm
Rotor slot number	8	Rotor outer diameter	50mm
Stator slot number	6	Air gap length	1mm
Stack length	80mm	PM thickness	3mm
Turns per AC coil	160	PM remanence	1.15T
Turn ratio of dc to ac winding	0.5	Rated speed	1500rpm
Rated phase voltage	220V	Rated load	5Nm
Stator tooth slot opening ratio	0.2	Rated frequency	200Hz
Stator slot opening ratio	0.27	Rated ac winding current	5A

Under the given rated voltage, the electric field winding is connected with the flux enhancement current. The machine starts with rated load, and its dynamic response is shown in Fig. 12.

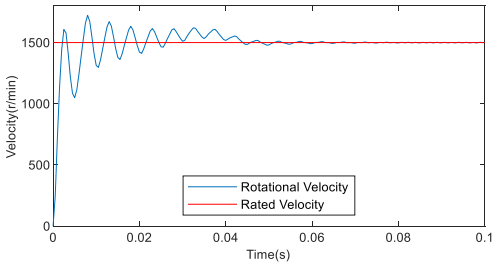

(a) Machine speed response

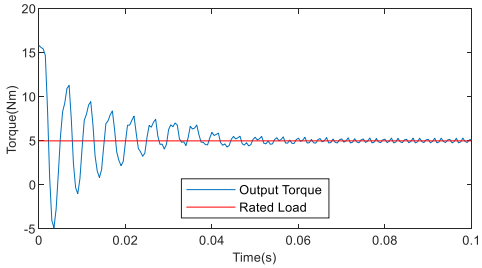

(b) Machine torque response

Fig. 12. Dynamic characteristics of machine.

From Fig. 12, it can be seen that the machine reaches steady state after 0.08 seconds. The machine efficiency is shown in Table 7.

Table 7: Rated efficiency of machine in machine state

Input Electromagnetic Power	1153.8W
Copper loss	92.6W
Core loss	43W
Machine efficiency	88.25%

When the control strategy of $i_d = 0$ is adopted. The angle between the phase current and the back EMF is kept at 0° by changing the excitation current without increasing the d-axis current component. Under the above conditions, Fig. 13 analyzes the relationship between voltage, output torque and speed, and the coupling relationship between field winding and power winding. As can be seen from Fig. 13 (a), when the excitation current is $-5A$(flux enhancing), the rated voltage can be reached as soon as possible. This is because the excitation current assists magnetism. Therefore, before reaching the rated speed, the output limit of the inverter voltage will be reached first. If the speed continues to increase, the main flux must be weakened by increasing the stator d-axis current. When the excitation current is 5A (flux weakening), the electric limit is reached when the rated speed is exceeded. This shows that with $i_d = 0$, the speed range can be increased just by adjusting the excitation current. As can be seen from Fig. 13 (b), when the excitation current is $-5A$ (flux enhancing), the output torque is 18% and 55% higher than the output torque when the excitation current is 0A and 5A, respectively. This shows that within a certain speed range, the overload capability of the machine can be greatly increased just by adjusting the excitation current.

The torque angle characteristic curve of HEFRM is shown in Fig. 14, and the corresponding torque angle is 90° when the control strategy of $i_d = 0$ is adopted. When the phase voltage of the machine is below the rated voltage, the torque angle can be kept at 90° for speed regulation. If the speed continues to increase, because the voltage output limit of the inverter has been reached, the voltage cannot continue to rise. The current angle is no longer zero, that is $i_d \neq 0$. The torque angle starts to increase and the output torque starts to decrease. At this time, the current angle is no longer zero, that is, $i_d \neq 0$, the torque angle begins to increase and the output torque begins to decrease. From the figure, it can be seen that in the process of increasing the torque angle, the torque output capacity can be improved by increasing the flux enhancement current, that is, the machine has higher overload capacity. From Fig. 15, it can be seen that under the condition of keeping the rated voltage unchanged, applying flux weakening current can significantly increase

the speed range of HEFRM compared to excitation with PMs separately.

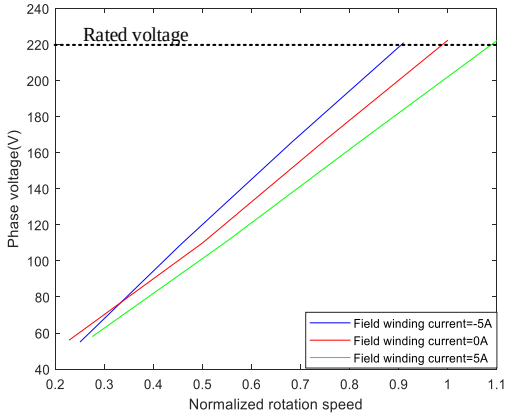

(a) Relationship between phase voltage and speed

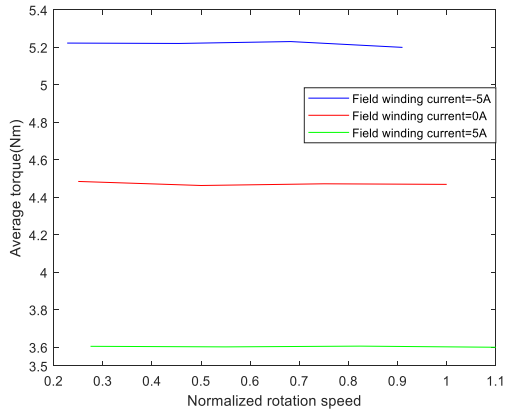

(b) Relationship between output torque and speed

Fig. 13. Comparison of relations under different excitation current .

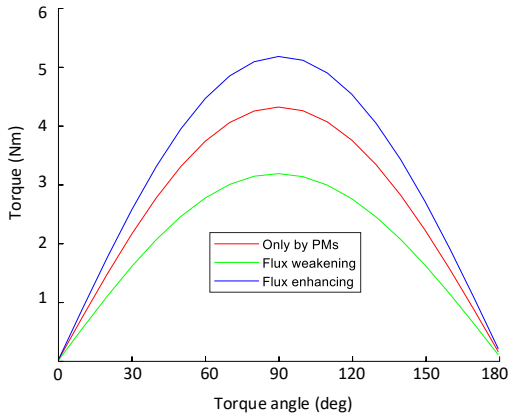

Fig. 14. Torque angle characteristic curve.

Figure 16 shows the comparison between the induced voltage the rated voltage of the field winding under different excitation currents. It can be seen that due to the new structure of the machine, the induced voltage of the field winding is almost zero when the flux enhancement and flux weakening currents are applied. This brings great convenience to the control of the field winding current.

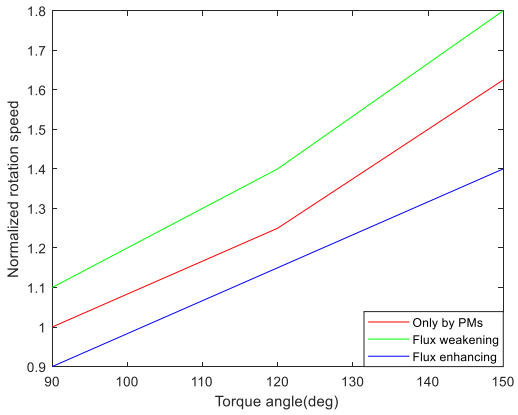

Fig. 15. Torque angle speed relationship (rated voltage).

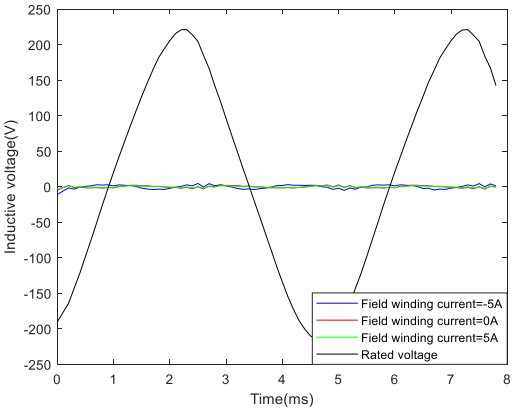

Fig. 16. Relationship between induced voltage and rated voltage of field winding.

V. CONCLUSION

This paper presents a novel hybrid excitation flux reversal machine. Compared with the traditional flux reversal machine, this structure has three advantages. First, the DC field winding is not placed in the stator slot, thus it will not occupy the stator slot area with the armature winding. Second, the DC field winding is decoupled from the armature winding, which is convenient to the control of the excitation current. Third, reasonable design of slot opening ratio of stator tooth slot can reduce torque ripple. When the genetic algorithm is applied for multi-objective optimization of the machine, we found that the optimal torque performance is obtained with stator tooth slot opening ratio of 0.2, stator slot opening ratio of 0.27, and rotor slot opening ratio of 0.58. Finally, under the control strategy of $i_d = 0$, it is

validated that a wider speed range and better overload capability can be achieved just by adjusting the excitation current.

ACKNOWLEDGMENT

This work was supported by the Natural Science Foundation of Jiangsu Province Grant No. BK20190634.

REFERENCES

[1] C. X. Wang, I. Boldea, and S. A. Nasar, "Characterization of three phase flux reversal machine as an automotive generator," [J]. *IEEE Transactions on Energy Conversion*, vol. 16, no. 1, pp. 74-80, Mar. 2001.

[2] V. Prakht, V. Dmitrievskii, V. Klimarev, and D. Askerov, "High speed flux reversal motor for power tool," [C]. *2016 6th International Electric Drives Production Conference (EDPC), IEEE*, pp. 306-311, Feb. 2017.

[3] W. Hua, X. Zhu, and Z. Wu, "Influence of coil pitch and stator-slot/rotor-pole combination on back EMF harmonics in flux-reversal permanent magnet machines," [J]. *IEEE Transactions on Energy Conversion*, vol. 33, no. 3, pp. 1330-1341, Jan. 2018.

[4] H. Yang, H. Lin, Z. Q. Zhu, H. Wang, S. Fang, and Y. Huang, "A novel flux-reversal hybrid magnet memory machine," [C]. *2017 IEEE Energy Conversion Congress and Exposition (ECCE), IEEE*, pp. 5853-5860, Nov. 2017.

[5] R. P. Deodhar, S. Andersson, I. Boldea, and T. J. Miller, "The flux-reversal machine: A new brushless doubly-salient permanent-magnet machine," *IEEE Transactions on Industry Applications*, vol. 33, no. 4, pp. 925-934, Aug. 1997.

[6] Z. Z. Wu and Z. Q. Zhu, "Partitioned stator flux reversal machine with consequent-pole PM stator," [J]. *IEEE Transactions on Energy Conversion*, vol. 30, no. 4, pp. 1472-1482, July 2015.

[7] C. Shi, R. Qu, B. Kou, D. Li, Y. Gao, and Y. Zhou, "A novel HTS flux-reversal linear permanent magnet machine with a lower number of mover teeth and higher thrust density," [J]. *IEEE Transactions on Applied Superconductivity*, vol. 28, no. 3, pp. 1-5, Jan. 2018.

[8] W. Li, K. T. Chau, T. W. Ching, and C. Liu, "A phase-decoupled flux-reversal linear generator for low-speed oscillatory energy conversion using impedance matching strategy," [J]. *IEEE Transactions on Industrial Electronics*, (99), 1-1, Jan. 2018.

[9] L. Xu, G. Liu, W. Zhao, J. Ji, and Z. Ling, "Analysis of new modular linear flux reversal permanent magnet motors," [J]. *IEEE Transactions on Magnetics*, vol. 51, no. 11, pp. 1-4, Nov. 2015.

[10] K. Xie, D. Li, R. Qu, and Y. Gao, "A novel permanent magnet vernier machine with Halbach array magnets in stator slot opening," [J]. *IEEE Transactions on Magnetics*, vol. 53, no. 6, pp. 1-5, June 2017.

[11] Y. Gao, D. Li, R. Qu, X. Fan, J. Li, and H. Ding, "A novel hybrid excitation flux reversal machine for electric vehicle propulsion," [J]. *IEEE Transactions on Vehicular Technology*, vol. 67, no. 1, pp. 171-182, Sep. 2017.

[12] D. Li, Y. Gao, R. Qu, J. Li, Y. Huo, and H. Ding, "Design and analysis of a flux reversal machine with evenly distributed permanent magnets," [J]. *IEEE Transactions on Industry Applications*, vol. 54, no. 1, pp. 172-183, Sep. 2017.

[13] Y. Gao, R. Qu, J. Li, J. Li, J. Li, and L. Wu, "Power factor of three-phase flux reversal machines," [C]. *2015 IEEE International Magnetics Conference (INTERMAG). IEEE*, 1-1, July 2015.

[14] M. Lin, G. Yang, and N. Li, "Overview of hybrid permanent magnet memory machine systems and their key technologies," Proceedings of the CSEE, vol. 38, no. 4, pp. 1187-1202, Feb. 2018. (in Chinese).

[15] Z. Z. Wu and Z. Q. Zhu, "Comparative analysis of end effect in partitioned stator flux reversal machines having surface-mounted and consequent pole permanent magnets," [J]. *IEEE Transactions on Magnetics*, vol. 52, no. 7, pp. 1-4, July 2016.

Xianming Deng was born in Sichuan, China. He received his B.S., M.S., and Ph.D. in Electrical Engineering from China University of Mining and Technology, Jiangsu, China. He is currently a Professor in the School of Electrical and Power Engineering of China University of Mining and Technology. His current research fields include power electronics and motor drive.

Zhen Jia was born in Xinjiang, China. He received his B.S. in Electrical Engineering from Chongqing University, Chongqing, China. He is currently receiving a Master education at China University of Mining and Technology. His current research interests include power electronics and motor drive.

Xiaohan Zhao was born in Shandong, China. She received her B.S. in Electrical Engineering from Shandong University of Technology, Shandong, China. She is currently receiving a Master education at China University of Mining and Technology. Her current research interests include power electronics and motor drive.